Preparation of Hollow Co_3O_4 Microspheres and Their Ethanol Sensing Properties

Qingze Jiao,[†] Min Fu,[†] Chao You,[‡] Yun Zhao,*,[†] and Hansheng Li[†]

[†]School of Chemical Engineering and the Environment, Beijing Institute of Technology, Beijing 100081, China
[‡]Patent Examination Cooperation Center of The Patent Office, Sipo, Beijing, China

ABSTRACT: The hollow Co_3O_4 microspheres were prepared by a gas−liquid diffusion reaction in the presence of ionic liquid [Bmim][BF$_4$] in combination with calcination at 300 °C. Their structures and morphologies were characterized by X-ray diffraction, scanning electron microscopy, transmission electron microscopy, Raman spectrometry, and X-ray photoelectron spectroscopy. The growth mechanism of hollow Co_3O_4 microspheres was proposed. The ethanol sensing properties were measured using a WS-30A gas sensor measurement system. The influence of working temperatures, ethanol concentrations, and specific surface areas of Co_3O_4 microspheres on the ethanol sensing properties was investigated. The hollow Co_3O_4 microspheres showed excellent sensitivity to ethanol vapor at a lower operating temperature.
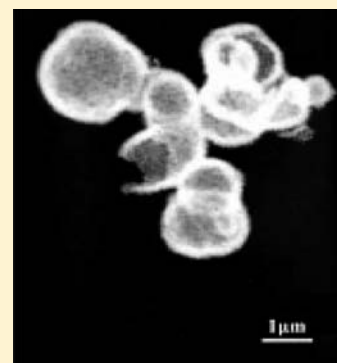
1. INTRODUCTION

As an important metal oxide ceramic material, Co_3O_4 has been paid intensive attention because of its excellent electrochemical performance,[1,2] efficient catalytic activity,[3,4] and outstanding magnetic properties[5−8] suitable for a wide range of applications. In recent years, Co_3O_4 has attracted general interest due to its good gas-sensing characteristics.[9] Sun et al.[10] prepared the nearly monodisperse Co_3O_4 nanocubes, and these nanocubes showed good gas sensing performance toward xylene and ethanol vapors with rapid and high responses at a low-operating temperature. Man et al.[11] reported the alcohol sensing behavior of Co_3O_4 nanostructures. The hollow Co_3O_4 nanorings showed the best sensitivity, and the sensitivity of porous Co_3O_4-like nanochains was superior to that of the porous nanosheets. Davide et al.[12] synthesized Co_3O_4-based nanosystems using plasma-enhanced chemical vapor deposition and investigated their gas sensing properties to ethanol and acetone. The results showed that an appreciable response improvement was dependent upon the fluorine content in the Co_3O_4 system. Lee et al.[13] described the synthesis of Co_3O_4 nanofibers and their gas sensing characteristics. The Co_3O_4 sensors prepared by heat treatment of as-spun precursor fibers at 500 and 600 °C showed well-developed one-dimensional morphologies and exhibited high responses to 100 ppm of C_2H_5OH at 301 °C with negligible cross-responses to 100 ppm of CO, C_3H_8, and H_2.

Hollow spheres with nanometer to micrometer dimensions represent an important class of material, because their unique structural, optical, and surface properties may lead them to a wide range of application, such as capsule agents for drug delivery, filters, coatings, chemical catalysis, gas sensors, or templates for functional architecture composite materials.[14−17] The synthesis of hollow spheres with certain morphologies has

become a hot topic in the field of inorganic materials. Various methods are used to synthesize hollow spheres, such as a hydrothermal reaction,[18] solvothermal technology,[19,20] the hard- and soft-templating method,[21,22] the self-assembly route,[23] the spray pyrolysis reaction,[24] and the sol−gel method.[25] However, the gas−liquid diffusion method is rarely used to prepare hollow spheres. It has the advantages of lower energy consumption and mild reaction conditions.

Green chemistry has become a tendency of chemical development in the 21st century. Because of nonvolatility, outstanding dissolution performance, and structural designability, the ionic liquid has unique advantages in the preparation of micronano materials. Li et al.[26] synthesized hollow CdS spheres with a diameter of 130 nm using a hydrothermal reaction in the presence of ionic liquid [Bmim][PF$_6$]. Duan et al.[27] synthesized hollow $MnCO_3$ spheres with a diameter of 1.5 μm via an ionic liquid-assisted hydrothermal route.

Herein, hollow Co_3O_4 spheres were obtained using a gas−liquid diffusion method in the presence of ionic liquid, followed by calcination. To the best of our knowledge, there has been no report of fabrication of hollow Co_3O_4 spheres using ionic liquid. As-prepared hollow products exhibited excellent sensitivity to ethanol vapor, showing potentials in sensors and related nanodevices.

2. EXPERIMENTAL SECTION

Materials. Ethanol, ammonium carbonate, and cobalt nitrate were purchased from the Chemical Reagent Company of Beijing. [Bmim][BF$_4$] was obtained from the Process Engineering Research Institute of the Chinese Academy of

Sciences. All chemical reagents were of analytical grade and used without further purification. All glassware (beakers and Petri dishes) was cleaned and sonicated in ethanol for 10 min, then rinsed with deionized water, and finally dried in the air. The reference air was purchased from Beijing Huaneng Specialty Gases Co., Ltd. It consists of 21% oxygen and 79% nitrogen, and the purity is 99.999%. The organic contaminants level was <2 × 10⁻⁶; the humidity level was <5 × 10⁻⁶.

2.1. Preparation and Characterization of Hollow Co₃O₄ Microspheres. In a typical experimental process, 10 mL of aqueous solution of $Co(NO_3)_2 \cdot 2H_2O$ (1 mM) was freshly prepared in the mixture of ionic liquid and deionized water with vigorous stirring, in the isotope bottle with a volume of 20 mL. The isotope bottle was then covered with a parafilm, which was punched with three needle holes and placed in a larger desiccator. One Petri dish containing crushed ammonium carbonate (3 g) was also covered with a parafilm punched with four needle holes and placed at the bottom of the desiccator. After 24 h, the parafilm was removed, and the precipitate on the bottom of the isotope bottles was rinsed with deionized water and ethanol and allowed to dry at room temperature. As-synthesized precursors were calcined at 300 °C for 2 h to obtain crystalline Co_3O_4. A schematic representation of the experimental setup is shown in Figure 1.
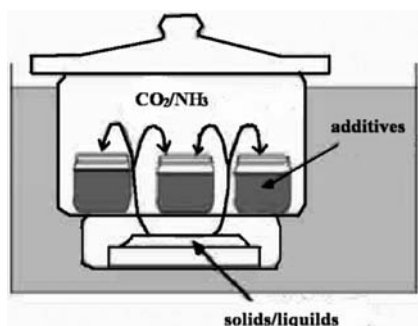
Figure 1. Schematic representation of the gas—liquid diffusion experimental setup.

Powder X-ray diffraction (XRD) patterns were recorded on a SHIMADZU-6000 X-ray diffractometer with Cu Kα radiation (λ = 1.54056 Å). The field emission scanning electron microscopy (FESEM) testing was performed with a HITACHI S-4800 microscope at an accelerating voltage of 15 kV. Transmission electron micrographs (TEM) were obtained using a Hitach-800 microscope at an accelerating voltage of 100 kV. The Raman spectrum was measured using a Renishaw inVia-Reflex Raman spectrometer. The X-ray photoelectron spectroscopy (XPS) testing was carried out at room temperature with Mg K_α radiation (hν = 1253.6 eV).

2.2. Fabrication and Analysis of Gas Sensors. Fabrication of the gas sensor was similar to the reported literature.[10,12,21,28−30] The hollow Co_3O_4 spheres were mixed with hydroxymethyl cellulose (CMC) binder to form a slurry and then pasted onto a ceramic tube (Al_2O_3) to form a thin film between two Au electrodes, which were previously printed on the ceramic tube and were connected with four platinum wires. The thickness of the electrodes was about 12 μm. The space between the electrodes was 2 mm, and the geometry of the electrodes was ribbon. The thickness of Co_3O_4 was required to be uniform, and its coverage was 100%. A structural schematic illustration of the gas sensor is shown in Figure 2, and a photograph of the gas sensor is shown in Figure 3.

A schematic presentation of the testing principle of the gas sensor is shown in Figure 4. The loop voltage and reference resistance are kept constant; the load voltage can be tested, so the gas sensor resistance can be obtained with the following formula:

$$R_S = \frac{V_C R_L}{V_{RL}} - R_L \tag{a}$$

The gas-sensing properties were measured using a WS-30A gas sensor measurement system. It consists of a PC, gas distribution chamber, sensing platform with a gas sensor, and cables. A schematic diagram of the sensing platform is shown in Figure 5. The gas distribution chamber was 300 mm × 300 mm × 200 mm; the volume was 18 000 mL. The measurement power, V_c, was 1.5−10 V. The reference resistance, R_L, was 510 Ω, 1 kΩ, 4.7 kΩ, 10 kΩ, 47 kΩ, 100 kΩ, 1 and MΩ. The sensor
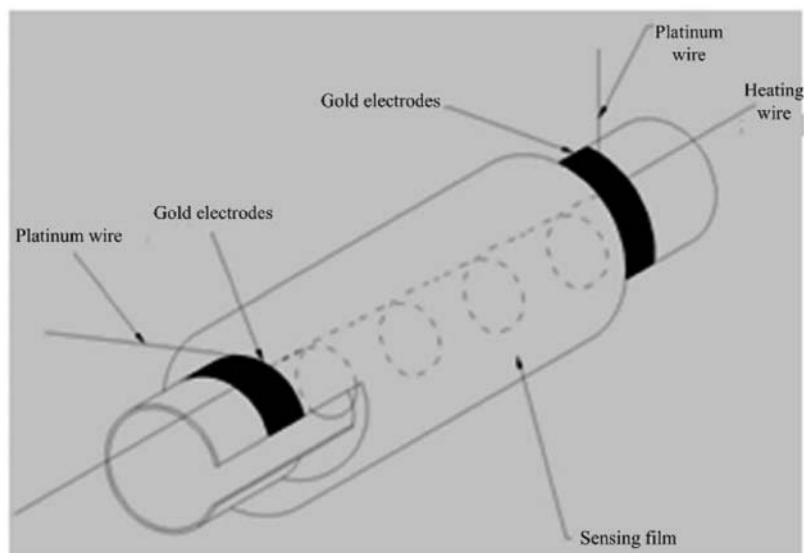
Figure 2. Structural schematic illustration of the gas sensor.

Figure 3. Photograph of the gas sensor.
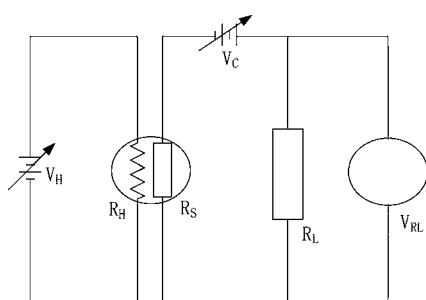
Figure 4. Schematic presentation of the testing principle of the gas sensor.
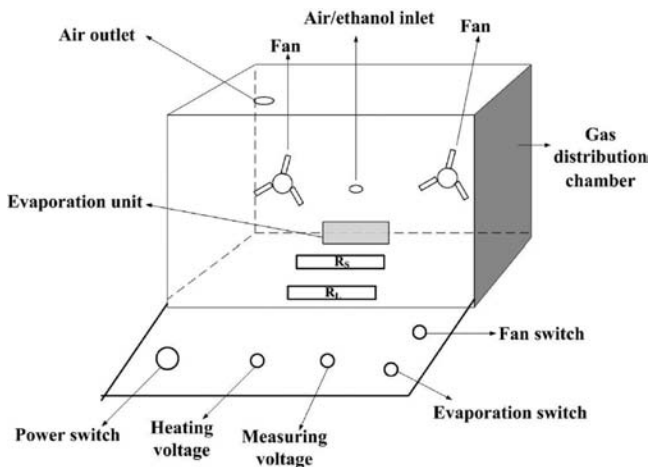
Figure 5. Schematic diagram of the sensing platform.

resistance is denoted as R_S. The operating temperature of the sensor was controlled by regulating the voltage of the heating wire. A static distribution method was utilized to control the concentration of ethanol. First, the reference air in a steel cylinder was introduced continuously (50 mL/min) into the gas distribution chamber by flow to replace the air in the chamber, and this process continued for 10 min. After the introduction of reference air was stopped, a trace of ethanol was taken using a trace sampler, injected into the evaporation unit in the gas distribution chamber, and heated to evaporation. Finally, the ethanol vapor was mixed with the reference air completely by a built-in fan. The different concentrations and

quality assurance of ethanol were obtained using the amount of ethanol in the trace sampler.

3. RESULTS AND DISCUSSION

3.1. The Morphologies and Structures of Co_3O_4. The structure of Co_3O_4 was determined by XRD. As shown in Figure 6a, all the diffraction peaks of the sample can be readily indexed as pure face-centered cubic Co_3O_4 (JCPDS card no. 80−1541).

Because Raman scattering is very sensitive to the microstructure of nanocrystalline materials, it was also used here to clarify the structure of the hollow Co_3O_4 spheres. As shown in Figure 6b, the Raman spectrum of the hollow Co_3O_4 microspheres shows five obvious Raman peaks located at around 184, 465, 510, 602, and 669 cm^{-1}, corresponding to all five of the Raman-active modes (F_{2g}, E_g, F_{2g}, F_{2g}, and A_{1g}) of Co_3O_4.

The chemical states of elements in Co_3O_4 were further investigated using XPS. Figure 6c shows the $Co2p_{3/2}$ and $Co2p_{1/2}$ peaks at 781.4 and 796.3 eV, respectively. As shown in Figure 6d, the O1s peaks at 528.8 and 530.2 eV can be attributed to Co^{2+}−O and Co^{3+}−O, respectively.[31−33] All the above characteristics confirm that the product is pure Co_3O_4.

The morphology and microstructure of the Co_3O_4 microspheres were investigated using SEM and TEM. As shown in Figure 7a, b, d, and f, the products exhibit a sphere-like morphology with a diameter of 1−3 μm. Damaged areas in Figure 7c, e, g, and i indicate hollow structures of products prepared in the presence of ionic liquids. It can be seen from Figure 7g that the walls of the hollow spheres have a uniform thickness of about 200 nm. With increasing concentration of ionic liquid, Co_3O_4 microspheres show a broader size distribution, and the number of damaged hollow microspheres increases.

Figure 8a and b show TEM images of Co_3O_4 microspheres synthesized in pure water, and Figure 8c, d, and e give TEM images of Co_3O_4 microspheres obtained in the mixture of water and [Bmim][BF$_4$]. It is obvious that Co_3O_4 microspheres obtained in pure water are solid. However, hollow and solid Co_3O_4 microspheres are all present for samples prepared in the presence of ionic liquid, and the number of hollow Co_3O_4 microspheres increases with increasing concentration of ionic liquid based on our observation.

Figure 9 shows nitrogen adsorption−desorption isotherms and pore-size distributions for the Co_3O_4 microspheres prepared with different volume ratios of H$_2$O to [Bmim][BF$_4$]. All samples showed a IV isotherm, indicating mesoporous structures and a narrow pore size distribution. In addition, Co_3O_4 microspheres give an extremely narrow pore size distribution centered around 4−6 nm in the mesopore region. As shown in Table 1, the average pore diameter decreases and the specific surface area of Co_3O_4 microspheres increases with increasing concentration of the ionic liquid.

3.2. Formation Mechanism of Hollow Co_3O_4 Microspheres. The mixture of ionic liquid and water is a complicated system. In general, the pure ionic liquid can form an "extended" hydrogen bond among the molecules in the liquid state. Koga et al.[34] found that when the concentration of [Bmim][BF$_4$] is higher than critical concentration, the ionic liquid starts associating and forms a cluster. Jiang et al.[35] synthesized flower-like Bi$_2$S$_3$ using a hydrothermal method, using a mixture of ionic liquid [Bmim][BF$_4$] and water as a medium. Vesicle clusters obtained from the ionic liquid and
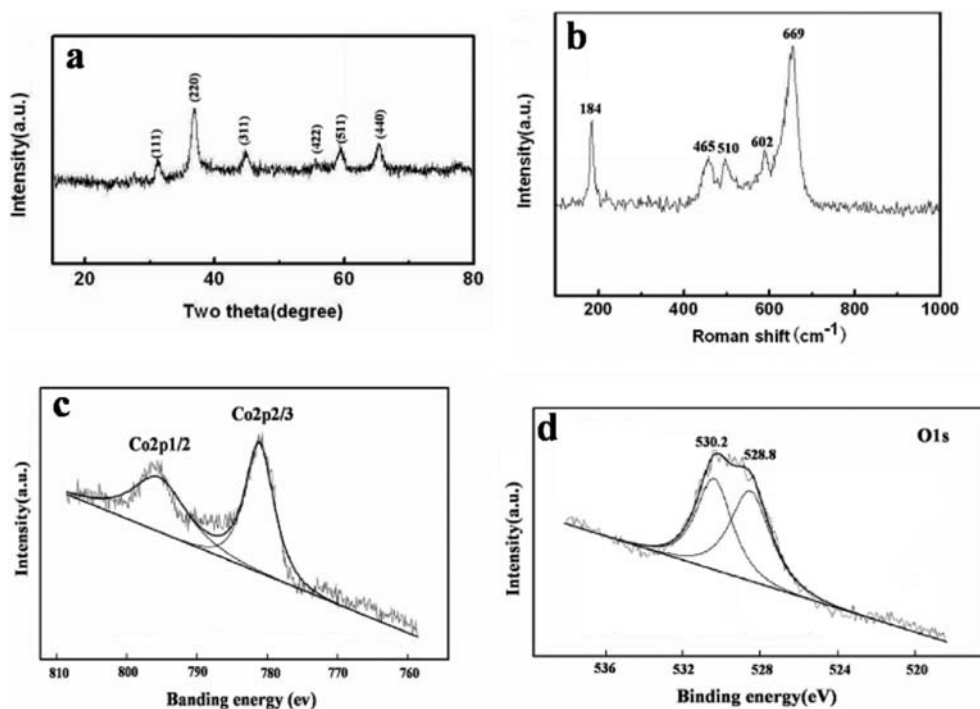
Figure 6. Co_3O_4 microspheres: (a) XRD pattern, (b) Raman spectrum, (c) $Co2p_{3/2}$ and $Co2p_{1/2}$ peaks of XPS survey scan, (d) O1s peaks of XPS survey scan.
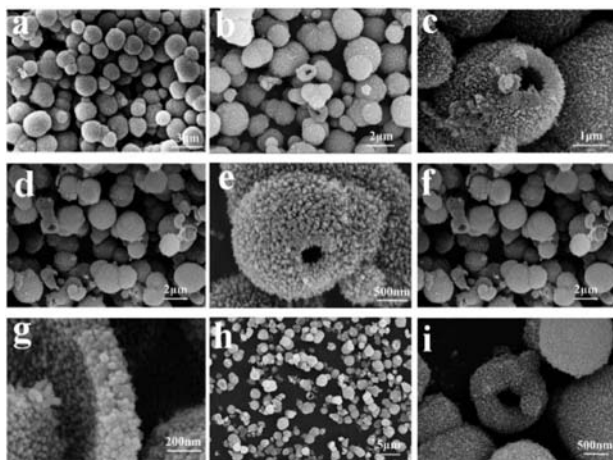
Figure 7. SEM images of Co_3O_4 microspheres obtained with different volume ratios of H_2O to [Bmim][BF_4]: (a) pure water; (b, c) 9:1; (d, e) 8:2; (f, g) 7:3; (h, i) 5:5.

Figure 8. TEM images of Co_3O_4 microspheres obtained in (a,b) pure water and (c, d, e) a mixture of water and ionic liquid.

water were observed. They were considered to be the template of a flower-like structure. Therefore, we speculated that similar vesicle clusters formed in our system. The surface of vesicle clusters was a hydrophilic BF_4 ion, and there were electrostatic interactions between Co^{2+} and the vesicle surfaces. With the introduction of ammonia, nucleation was performed on its surface. Particles gradually grew and connected to each other and finally formed a shell with ionic liquid inside and outside. After calcination, hollow Co_3O_4 microspheres were obtained with decomposition of the ionic liquid. The possible growth mechanism diagram of hollow microspheres is shown in Figure 10.

3.3. Ethanol Sensing Properties of Hollow Co_3O_4 Microspheres.
As an important chemical with a wide range of applications, ethanol is flammable and explosive. Ethanol

leakage in industrial production processes may cause fires, explosions, and other potential dangers. There is a demand for online detection of ethanol in industry, security, and environmental monitoring. Additionally, gas sensors based on ethanol-sensing materials can be used to detect ethanol vapor concentrations in the driver's exhaled breath in order to prevent drunk driving and reduce traffic accidents. Therefore it is necessary to find excellent ethanol sensing materials.

3.3.1. Ethanol Sensing Properties of Hollow Co_3O_4 Microspheres with Different Ethanol Concentrations. The gas response is defined as the ratio of the stationary electrical resistance of the sensor in the test gas (R_g) and in the air (R_a), i.e., $S = R_g/R_a$. The comparative response versus ethanol concentration of the hollow Co_3O_4 microspheres obtained with a volume ratio of 5:5 for H_2O to [Bmim][BF_4] is shown in
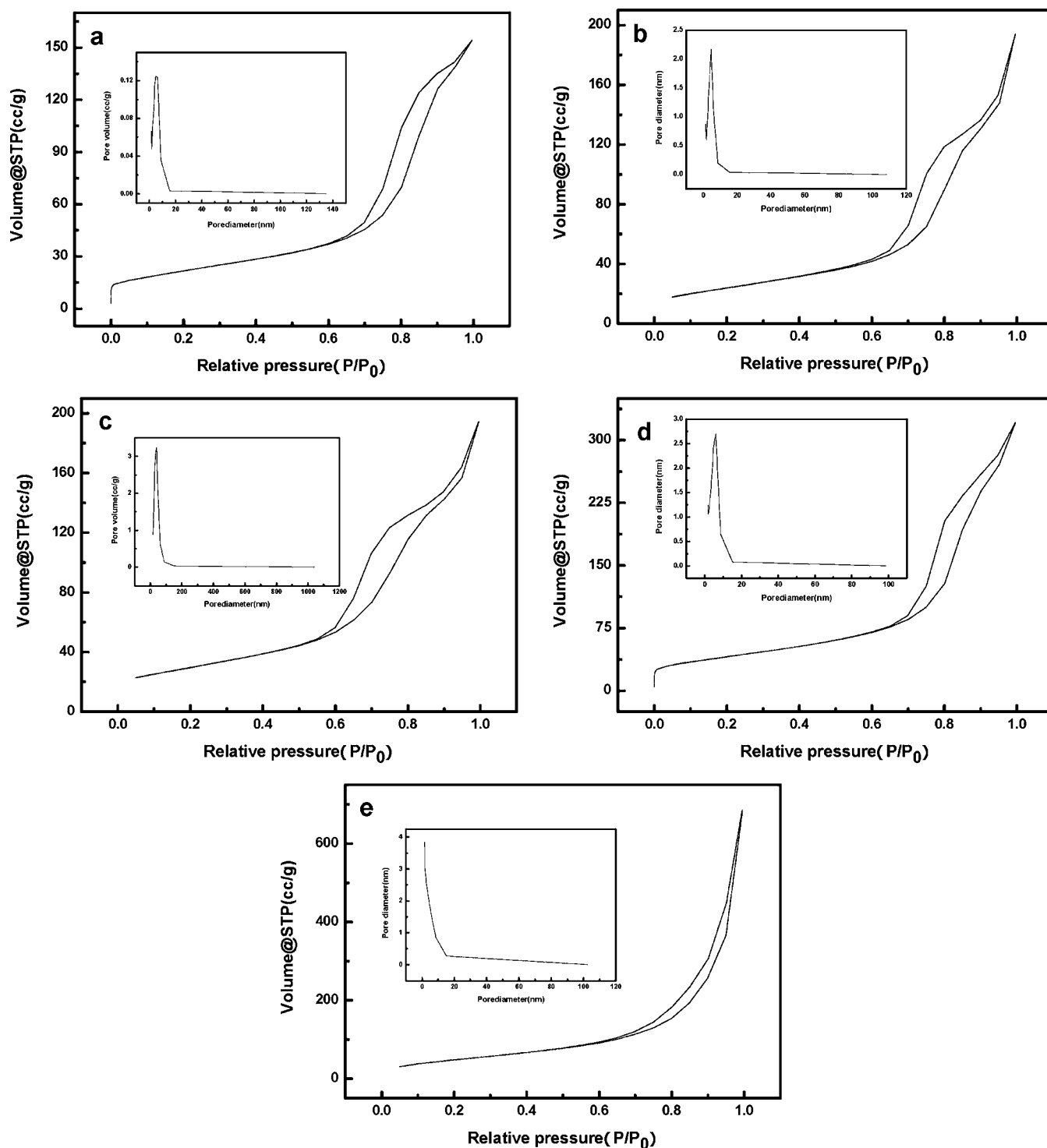
Figure 9. Nitrogen adsorption−desorption isotherm and pore-size distribution for the Co_3O_4 microspheres prepared with different volume ratios of H_2O to $[Bmim][BF_4]$: (a) pure water, (b) 9:1, (c) 8:2, (d) 7:3, (e) 5:5.

Table 1. Surface Areas and Average Pore Diameters for Co_3O_4 Microspheres Prepared with Different Volume Ratios of H_2O to $[Bmim][BF_4]$

	$H_2O/[Bmim][BF_4]$				
	pure water	9:1	8:2	7:3	5:5
S_{BET} /$m^2 \cdot g^{-1}$	73.25	96.57	118.31	145.79	183.5
D_d /nm	6.19	5.06	4.76	4.38	4.15

Figure 11. The response to ethanol is 10 and 45 at concentrations of 10 and 1000 ppm, respectively. It was also found that the relative sensitivity increases with increasing the ethanol concentration. Furthermore, the hollow Co_3O_4 microsphere-based sensor exhibits a linear response to ethanol in the range of 10−1000 ppm.

3.3.2. Optimum Working Temperature for the Gas Sensor. Temperature is an important factor to affect the performance of gas sensors. Figure 12 presents an ethanol sensing curve (500
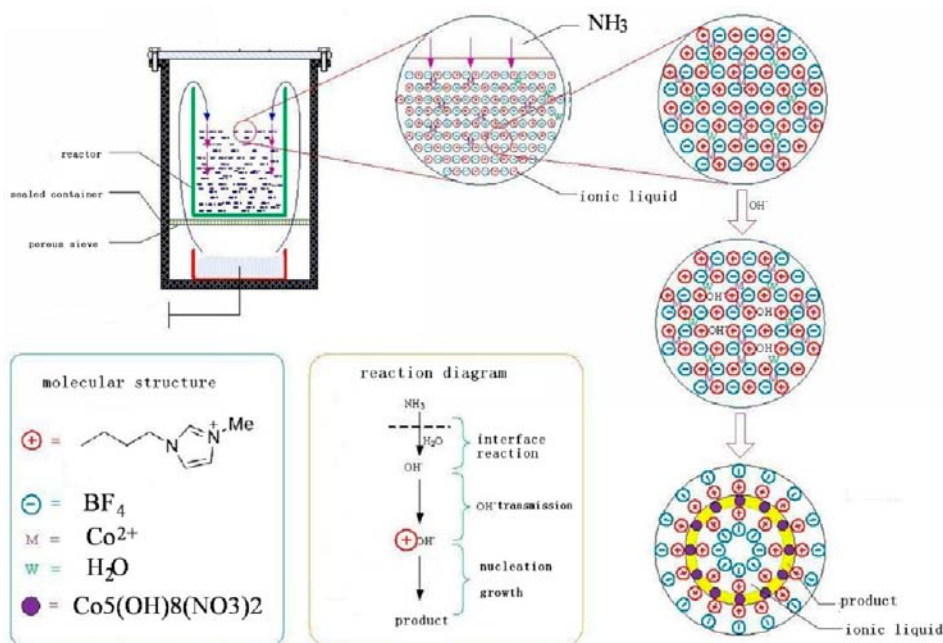
Figure 10. The growth mechanism diagram of hollow microspheres.
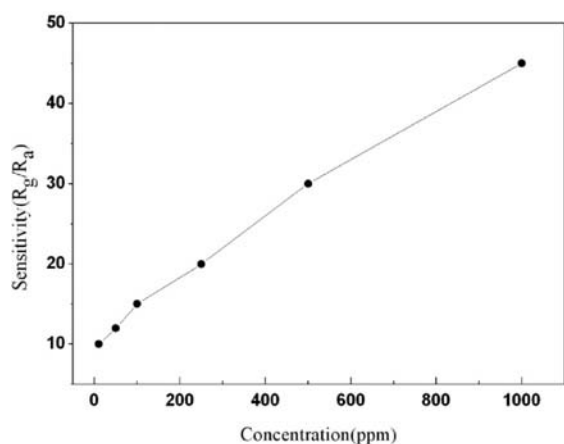
Figure 11. Sensor response of Co_3O_4 microspheres with different ethanol concentrations at 180 °C.
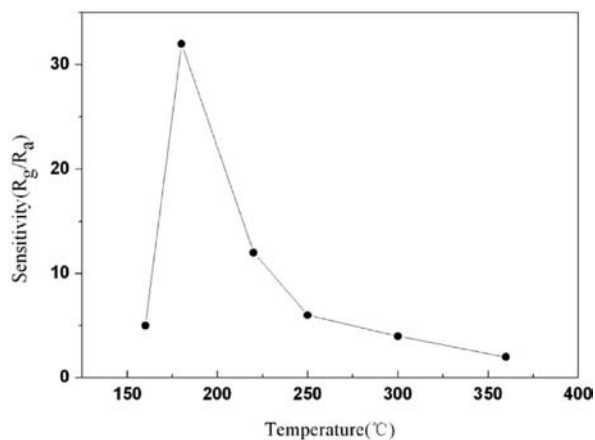
Figure 12. Gas responses versus operating temperatures of hollow Co_3O_4 microspheres to 500 ppm of ethanol.

ppm of ethanol) of hollow Co_3O_4 microspheres obtained with a volume ratio of 5:5 for H_2O to $[Bmim][BF_4]$, at different working temperatures of 160, 180, 220, 250, 300, and 370 °C. Samples show great sensitivity to ethanol at 180 °C, indicating that the optimum working temperature of hollow Co_3O_4 microspheres is 180 °C.

3.3.3. Response-Recovery Characteristics. Response-recovery characteristics are a key indicator for gas sensors. Figure 13
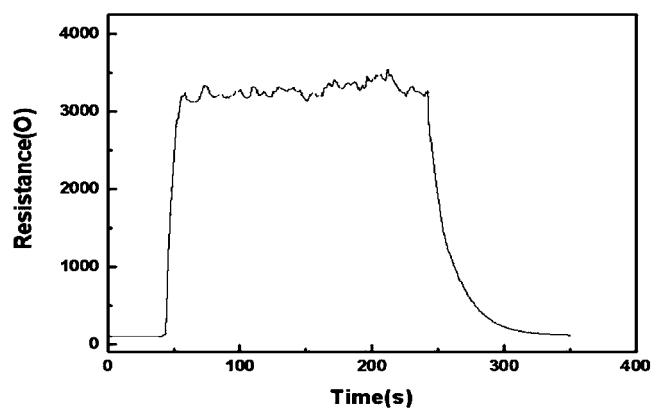
Figure 13. Response and recovery of hollow Co_3O_4 microspheres to 500 ppm of ethanol at 180 °C.

presents a typical response curve when hollow Co_3O_4 microspheres obtained with a volume ratio of 5:5 for H_2O to $[Bmim][BF_4]$, were exposed to 500 ppm of ethanol at 180 °C. The response of the hollow Co_3O_4 microsphere based sensors increases quickly and drops rapidly. The response and recovery times were 6 and 22 s, respectively, indicating a fast adsorption−desorption rate and a good response capability to ethanol.

3.3.4. Ethanol Sensing Properties of Different Co_3O_4 Hollow Microspheres. Figure 14 illustrates the sensitivity of Co_3O_4 microspheres prepared with different volume ratios of H_2O to $[Bmim][BF_4]$. Figure 15 illustrates the gas-sensing
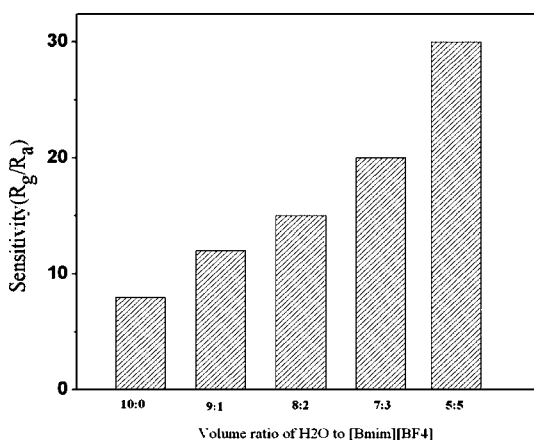
Figure 14. Sensitivity of Co_3O_4 obtained from different volume ratios of H_2O to $[Bmim][BF_4]$.
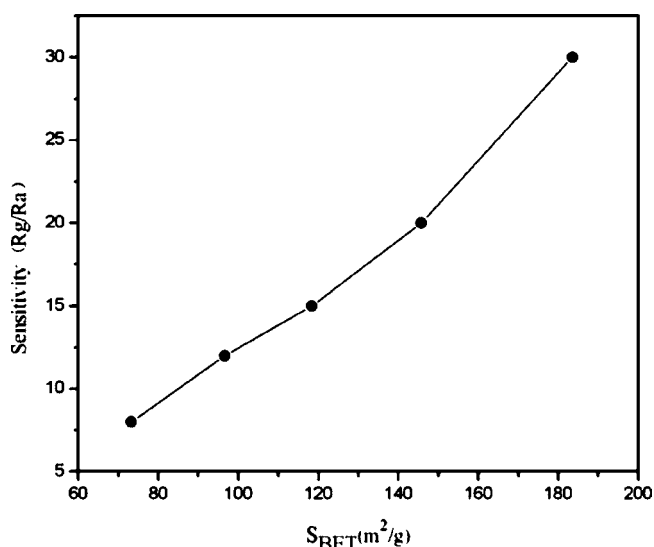
Figure 15. Ethanol sensing properties of Co_3O_4 microspheres with different specific surface areas.

behavior of Co_3O_4 microspheres with different specific surface areas in the presence of ethanol. It is clear that the hollow Co_3O_4 microsphere-based sensor shows better sensitivity to ethanol than that of solid ones, and the sensitivity of hollow Co_3O_4 microspheres to ethanol increases as the concentration of ionic liquid increases. The sensitivity of solid Co_3O_4 microspheres obtained in pure water is only 8, while the sensitivity increases to 30 when the volume ratio of H_2O to $[Bmim][BF_4]$ is 5:5. The gas-sensing action occurs on the surface of the gas sensor. The increase of specific surface area can lead to more active sites emerging on the surface for chemical or physical interactions, thereby enhancing the gas adsorption and accelerating the gas-sensing action. In this case, ethanol vapor can adsorb and desorb quickly from hollow Co_3O_4 microspheres.[36,37] Therefore it can be concluded that the specific surface area plays an important role in the sensitivity test for ethanol: the larger the specific surface area, the higher the sensitivity.[38,39]

4. CONCLUSION

In conclusion, hollow Co_3O_4 spheres were successfully synthesized in the presence of ionic liquid $[Bmim][BF_4]$ and

water, using a facile gas−liquid diffusion method followed by calcination. The hollow Co_3O_4 microsphere-based sensors show better sensitivity to ethanol than that of solid ones, and they exhibit excellent sensitivity to ethanol vapor at 180 °C. The hollow Co_3O_4 microspheres exhibit a linear response to ethanol in the range of 10−1000 ppm. As the specific surface area of Co_3O_4 microspheres increases, their sensitivity goes higher. The use of ionic liquid in micronano materials using the gas−liquid diffusion method offers new insights into controlling the structure and morphology under easily attainable reaction conditions.

■ AUTHOR INFORMATION

Corresponding Author

*E-mail: zhaoyun@bit.edu.cn.

Notes

The authors declare no competing financial interest.

■ REFERENCES

(1) Chuan, L.; James, A.; Branko, N. *J. Electrochem. Soc.* **1998**, *145*, 4097−4101.
(2) Lou, X. W.; Deng, D.; Lee, J. Y.; Feng, J.; Archer, L. A. *Adv. Mater.* **2008**, *20*, 258−262.
(3) Natile, M. M.; Glisenti, A. *Chem. Mater.* **2002**, *14*, 3090−3099.
(4) Jansson, J.; Palmqvist, A. E. C.; Fridell, E.; Skoglundh, M.; Österlund, L.; Thormählen, P.; Langerc, V. *J. Catal.* **2002**, *211*, 387−397.
(5) Cao, A. M.; Hu, J. S.; Liang, H. P.; Wan, L. J. *J. Phys. Chem. B* **2006**, *110*, 15858−15863.
(6) Wang, G. X.; Shen, X. P.; Horvat, J.; Park, J. *J. Phys. Chem. C* **2007**, *111*, 163−167.
(7) Wolf, A.; Schüth, F. *Appl. Catal., A* **2002**, *226*, 1−13.
(8) Makhlouf, S. A. *J. Magn. Magn. Mater.* **2002**, *246*, 184−190.
(9) Choia, K.; Kima, H. R.; Kim, K. M.; Liu, D.; Cao, G. Z.; Lee, J. H. *Sens. Actuators, B* **2010**, *146*, 183−189.
(10) Sun, C.; Su, X. T.; Xiao, F.; Niu, C.; Wang, J. *Sens. Actuators, B* **2011**, *157*, 681−685.
(11) Man, L. Y.; Niu, B.; Xu, H. Y. *Mater. Res. Bull.* **2011**, *46*, 1097−1101.
(12) Davide, B.; Daniela, B.; Elisabetta, C.; Anjana, D.; Roland, A. F.; Alberto, G.; Marco, G.; Chiara, M.; Cinzia, S.; Giorgio, S.; Eugenio, T. *Sens. Actuators, B* **2011**, *160*, 79−86.
(13) Yoon, J. W.; Choi, J. K.; Lee, J. H. *Sens. Actuators, B* **2012**, *161*, 570−577.
(14) Zeng, H. C. *J. Mater. Chem.* **2006**, *16*, 649−662.
(15) Jeong, U.; Wang, Y.; Ibisate, M; Xia, Y. *Adv. Funct. Mater.* **2005**, *15*, 1907−1921.
(16) Sugama, T.; Lipford, B. *J. Mater. Sci. Technol.* **1997**, *32*, 3523−3534.
(17) Okada, K.; Shimai, A.; Takei, T.; Hayashi, S.; Yasumori, A.; MacKenzie, K. *Microporous Mesoporous Mater.* **1998**, *21*, 289−296.
(18) Shi, L.; Du, F. *Mater. Res. Bull.* **2007**, *42*, 1550.
(19) Li, Z.; Xie, Y.; Xiong, Y.; Zhang, R. *New J. Chem.* **2003**, *27*, 1518.
(20) Ashoka, S.; Chithaiah, P.; Thipperudraiah, K. V.; Chandrappa, G. T. *Inorg. Chim. Acta* **2010**, *363*, 3442−3447.
(21) Lai, X. Y.; Li, J.; Korgel, B. A.; Dong, Z. H.; Li, Z. M.; Su, F. B.; Du, J.; Wang, D. *Angew. Chem., Int. Ed.* **2011**, *50*, 2738−2741.
(22) Liang, C. D.; Hong, K.; Guiochon, G. A.; Mays, J. M.; Dai, S. *Angew. Chem., Int. Ed.* **2004**, *43*, 5785−5789.
(23) Wang, X.; Wu, X.; Guo, Y. *Adv. Funct. Mater.* **2010**, *20*, 1680.
(24) Hong, S-H; Kim, B.-K. *Mater. Lett.* **2003**, *57*, 2761−2767.

(25) Zhong, J.; Liang, S. Q.; Zhao, J.; Wu, W. D.; Liu, W. J.; Wang, H. T.; Chen, X. D.; Cheng, Y. B. *J. Eur. Ceram. Soc.* **2012**, *32*, 3407−3414.

(26) Li, X. P.; Gao, Y. N.; Yu, L.; Zheng, L. Q. *J. Solid State Chem.* **2010**, *183*, 1423−1432.

(27) Duan, X. C.; Lian, J. B.; Ma, J. M.; Kim, T.; Zheng, W. J. *Cryst. Growth Des.* **2010**, *10*, 4449−4455.

(28) Jing, Z. H.; Zhan, J. H. *Adv. Mater.* **2008**, *20*, 4547−4551.

(29) Li, Z. M.; Lai, X. Y.; Wang, H.; Mao, D.; Xing, C. J.; Wang, D. *J. Phys. Chem. C* **2009**, *113*, 2792.

(30) Lai, X. Y.; Wang, D.; Han, N.; Xing, C. J.; Li, Z. M. *Chem. Mater.* **2010**, *22*, 3033−3042.

(31) Xu, R.; Zeng, H. C. *Langmuir* **2004**, *20*, 9780−9790.

(32) He, T.; Chen, D. R.; Jiao, X. L.; Wang, Y.; Duan, Y. Z. *Chem. Mater.* **2005**, *17*, 4023−4030.

(33) Cong, H. P.; Yu, S. H. *Cryst. Growth Des.* **2009**, *9*, 210−217.

(34) Katayanagi, H.; Nishikawa, K.; Shimozaki, H.; Miki, K.; Westh, P.; Koga, Y. *J. Phys. Chem. B.* **2004**, *108*, 19451−19457.

(35) Jiang, J.; Yu, S. H.; Yao, W. T.; Ge, H.; Zhang, G. Z. *Chem. Mater.* **2005**, *17*, 6094−6100.

(36) Choi, K I.; Kim, H. R.; Lee, J. H. *Sens. Actuators, B* **2009**, *138*, 497−503.

(37) Xua, J. Q.; Jia, X. H.; Lou, X. D.; Xi, G. X.; Han, J. J.; Gao, Q. H. *Sens. Actuators, B* **2007**, *120*, 694−699.

(38) Ansari, Z. A.; Ansari, S. G.; Ko, T.; Oh, J. H. *Sens. Actuators, B* **2002**, *87*, 105−114.

(39) Patil, D.; Patil, P.; Subramanian, V.; Joy, P. A.; Potdar, H. S. *Talanta* **2010**, *81*, 37−43.